RSC Advances

PAPER

View Article Online
View Journal | View Issue

Check for updates

Cite this: *RSC Adv.*, 2021, **11**, 30689

Isostructural cocrystals of metaxalone with improved dissolution characteristics†

Sunil Kumar Gohel,[a] Vasanthi Palanisamy,[b] Palash Sanphui,[b]* Muthuramalingam Prakash,[b] Girij Pal Singh[a] and Vladimir Chernyshev*[cd]

Muscle relaxant and pain reliever metaxalone (MET) is a biopharmaceutical classification systems (BCS) class II drug with poor aqueous solubility and high permeability. The presence of an aromatic skeleton and cyclic carboxamate moiety are the probable reasons for the decreased aqueous solubility, which impacts on its low bioavailability. A high dose (800 mg) of the drug often creates adverse side effects on the central nervous system that needs urgent remedy. Cocrystallization of MET with nicotinamide (NAM), salicylamide (SAM), and 4-hydroxybenzoic acid (HBA) resulted in multicomponent solids that were characterized by PXRD, DSC and single crystal X-ray diffraction. Cocrystals with SAM and NAM form 2D isostructural cocrystals, whereas with HBA the result is a differently packed cocrystal hydrate (or anisole hemisolvate) depending upon the crystallization medium. Similar to the reported MET cocrystals, these cocrystals also confirm the preference for an imide···imide homosynthon in the drug. The dominance of the drug–drug homodimer over drug-coformer heterodimers was demonstrated based on binding energy calculations. Further, powder dissolution experiments in pH 6.8 phosphate buffer indicate that the cocrystals improved the apparent solubility compared to the native drug by 3–9 fold. The absence of stronger heterosynthons between MET and the coformers, their lower melting points and the high solubility of the coformers are the probable reasons for the enhanced solubility of the bioactive component. The MET–NAM cocrystal exhibited the highest solubility/dissolution rate among the three binary solid forms, which may offer improved bioavailability and a lower dose with minimal side effects.

Received 6th August 2021
Accepted 9th September 2021

DOI: 10.1039/d1ra05959a

rsc.li/rsc-advances

Open Access Article. Published on 15 September 2021. Downloaded on 4/7/2026 1:42:27 PM.
This article is licensed under a Creative Commons Attribution-NonCommercial 3.0 Unported Licence.

Introduction

Pharmaceutical cocrystals involving an active ingredient with a generally regarded as safe (GRAS) molecule offer tuning of drug properties ranging from solubility, permeability and bioavailability to clinical efficacy.[1] Following the regulatory approval from US-FDA (2013, 2018) and EMA (2015), four pharmaceutical cocrystals (ipragliflozin–L-proline, ertugliflozin–L-pyroglutamic acid, escitalopram–oxalate and chloral–betaine) and four drug–drug cocrystals (valproic acid and valproate sodium, valsartan sodium and sacubitril sodium, diphenhydramine and 8-chlorotheophylline, and Antipyrin and hypnotic chloral hydrate) have been commercialized till date.[1d] Many more cocrystals are in the research and development pipeline to enter into the market. Complying US-FDA guidelines, generic pharma industries need to ensure that the cocrystals must be dissociable and only the active ingredient needs to reach the target site.[2] Unlike suitability of salts to the ionized species, cocrystals are applicable for both neutral and ionic species.[3] Often cocrystals offer a dual advantage of solubility and stability compared to the other solid forms.[3a]

Isostructurility indicates different components with similar crystal packing. When closely related molecules like homologues or phenylogues are introduced in the crystal lattice of a single component, the corresponding binary system may exhibit close packing.[4] Isostructural cocrystals with similar structural blueprints may exhibit modified pharmaceutically relevant properties due to the presence of variable coformers and minor changes in their conformations and packing features. Often, isostructural cocrystals have similar lattice parameters including space groups, defined as isomorphs, which generally exhibit identical X-ray diffraction pattern.[4a,c] These cocrystals can be exploited to positively modify drug properties by substituting a suitable coformer without disturbing much of the crystal lattice similar to the concept of drug-biomolecule (enzyme, receptor) binding.

[a]*Lupin Limited, Lupin Research Park, Pune-412115, Maharashtra, India*

[b]*Department of Chemistry, Faculty of Engineering and Technology, SRM Institute of Science and Technology, Chennai, Tamil Nadu 603203, India. E-mail: palashi@srmist.edu.in*

[c]*Department of Chemistry, M. V. Lomonosov Moscow State University, 1-3 Leninskie Gory, Moscow 119991, Russian Federation. E-mail: vladimir@struct.chem.msu.ru*

[d]*A. N. Frumkin Institute of Physical Chemistry and Electrochemistry RAS, 31 Leninsky Prospect, Moscow 119071, Russian Federation*

† Electronic supplementary information (ESI) available: PXRD comparison, Rietveld plot of MET–NAM cocrystal, crystal structure packing of MET–SAM cocrystals, XPac derived 2D supramolecular constructs, DSC/TGA analysis of MET–HBA (anisole solvate). CCDC 2067490 and 2067491. For ESI and crystallographic data in CIF or other electronic format see DOI: 10.1039/d1ra05959a

© 2021 The Author(s). Published by the Royal Society of Chemistry

Open Access Article. Published on 15 September 2021. Downloaded on 4/7/2026 1:42:27 PM.
This article is licensed under a Creative Commons Attribution-NonCommercial 3.0 Unported Licence.

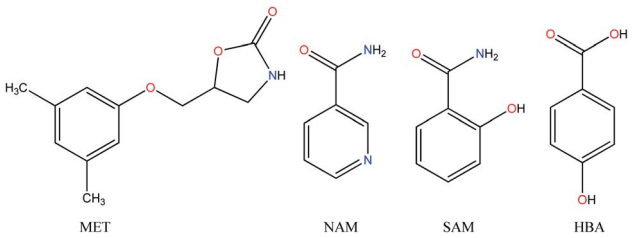

Fig. 1 Chemical diagrams of the native drug, metaxalone and coformers discussed in this study.

Metaxalone (chemical name: 5-[(3,5-dimethylphenoxy) methyl]-2-oxazolidinone, MET hereafter Fig. 1), is a medication to relief moderate to strong muscle pain caused by strains, sprains, and other musculoskeletal conditions.[5a] Its biological action involves depression of central nervous system. Poor solubility (91 mg L^{-1}) and high intestinal permeability (log *P* −2.3) of the drug falls in Biopharmaceutics Classification System (BCS) class II category.[5b] Poor bioavailable drug, MET is orally administered as 400 and 800 mg tablets under the brand name Skelaxin. High dose (dose no, D_0 35.2) of the drug provokes side effects of potential central nervous system particularly among the elder patients. MET tablets are generally prescribed to be consumed along with food to enhance its bioavailability. MET with non-ionizable functional groups like carboxamate does not favour salt formation. Hence, cocrystallization is one of the crystal engineering solution for the drug to improve its solubility and pharmacokinetics.

Racemic MET crystallized as dimorphic systems (Forms A and B), which are enantiotropically related.[6a] The recemic (R/S) Form A of MET is commercially available. Recently, Bredikhin *et al.* reported the crystal structure of pure S-MET, which is close to Rec-Form A.[6b] In addition, the drug is reported to constitute binary (1 : 0.5) cocrystals with dicarboxylic acids like maleic acid, fumaric acid, succinic acid, adipic acid and salicylic acid (1 : 1) in a patent and publication.[7] All these cocrystal structures have common motif of imide···imide homosynthon of MET that confirms quite strong homodimer of the native drug, which is difficult to break. In addition, MET forms lower melting cocrystals with salicylamide, nicotinamide, isonicotinamide, *meta*/*para*-hydroxybenzoic acids, out of which only MET–SAM cocrystal structure with MET–MET homodimer was reported by us.[8a] Lately, Aziz *et al.* reported two cocrystals of the drug with saccharin and lactic acid with improved dissolution rate.[8b] Those cocrystals were characterized by XRD, FT-IR, DSC and SEM images. To search for alternate solid forms with MET–coformer heterosynthon in order to enhance dissolution rate, the crystal structures of MET cocrystals with NAM and HBA were determined. The crystal structure of MET–NAM cocrystal was confirmed from high resolution XRD data, whereas MET–HBA cocrystal was structurally characterized using single crystal X-ray diffraction. In addition, dissolution experiments were carried out in pH 6.8 phosphate buffer medium to find out the suitable solid form with optimum solubility. NAM is a form of vitamin B that is used as a dietary supplement and also to treat pellagra.[9] SAM is often combined with aspirin and caffeine to treat as a pain relief drug.[10] Besides, anti-oxidant properties, HBA is also used as preservatives in the form of parabenes in cosmetics and in ophthalmic solution.[11] Due to the medicinal importance of the coformers, the corresponding cocrystals may be treated as drug–drug cocrystals that are highly demanding due to their synergistic effect in drug properties and clinical efficacy.[12]

Materials and methods

MET was procured from Lupin, Mumbai. Solvents were commercially available and used as received without further purification.

Preparation of cocrystals

MET–NAM (1 : 1). 221 mg MET (1 mmol) and 122 mg NAM (1 mmol) were ground in a mortar and pestle for 20 minutes using a few drops of acetone. The final solid ground material (50 mg) was dissolved in 2 ml acetone and left for slow evaporation. Because of unsuitable single crystals harvested from crystallization methods, corresponding cocrystal structure was determined using high resolution PXRD data. Melting point: 105–107 °C.

MET–HBA (1 : 1) hydrate/solvate. The binary cocrystal was prepared by grinding equimolar mixture of 221 mg MET (1 mmol) and 138 mg HBA (1 mmol) in a mortar and pestle for 20 minutes using a few drops of acetone. The ground material (50 mg) was dissolved in 2 ml methanol and left for slow evaporation. The very fine fibre like crystals (of hydrate) were obtained from acetone, which were not suitable for X-ray diffraction.[8a] Comparatively, diffraction quality needle crystals were harvested from anisole. In addition, the cocrystal was reproduced by anisole assisted grinding and slurry experiments of MET and HBA (1 : 1). Melting point: 115–117 °C.

Powder X-ray diffraction

Powder X-ray diffraction pattern of MET, coformer and their ground mixture were recorded on a PANalytical X'Pert Pro X-ray powder diffractometer. MET–HBA (1 : 1) anisole solvate was compared with the calculated X-ray patterns of its crystal structure, see Fig. S1, ESI.† Data collection was carried out at room temperature using Cu-Kα1 radiation (1.5418 Å; 40 kV, 30 mA) as X-ray source in 2θ continuous scan mode (Bragg–Brentano geometry) in the range of 5 to 50° at a scan rate of 1° min^{-1} and time per step 0.5 s.

Thermal analysis

DSC (differential scanning calorimetry) of ground sample (cocrystal) and the drug were performed on a Diamond DSC Perkin Elmer-10 module. 2–3 mg of each sample was placed in a crimped and vented aluminium sample pan and run at a heating rate of 10 °C min^{-1} under dry N_2 atmosphere. Enthalpy of fusion was calculated from the integration of the area of the melting peak and the interpolated baseline between the beginning and end of the endotherm. A PerkinElmer Pyris-1 TGA (Thermogravimetric analysis) instrument was employed by heating 10 mg sample of

© 2021 The Author(s). Published by the Royal Society of Chemistry

Open Access Article. Published on 15 September 2021. Downloaded on 4/7/2026 1:42:27 PM.
This article is licensed under a Creative Commons Attribution-NonCommercial 3.0 Unported Licence.

MET–HBA (anisole) solvate in an open aluminium crucible in the temperature range of 30–300 °C at 10° min^{-1}.

Crystal structure from PXRD data

The crystal structure of MET–NAM was determined from powder X-ray diffraction data measured at room temperature on the Guinier-Huber camera G670 with curved germanium monochromator (Cu-Kα1 radiation, $\lambda = 1.54059$ Å). The powder X-ray pattern was indexed in a triclinic unit cell. The crystal structure was solved in the space group $P\bar{1}$ with the use of simulated annealing technique and refined (Rietveld refinement) with the program MRIA following the known procedure described by us earlier.[13] All non-H atoms were isotropically refined. H atoms were placed in calculated positions and refined accordingly. The experimental and calculated diffraction profiles after the final bond-restrained Rietveld refinement are shown in Fig. S1, ESI.† The crystal data, data collection and refinement parameters are summarized in Table 1.

Single crystal X-ray diffraction

Good quality single crystals (acicular morphology) of MET–HBA cocrystal were harvested in anisole. One of the best quality single crystal was mounted on a Bruker APEX-II CCD with graphite monochromated Mo-Kα radiation ($\lambda = 0.71073$ Å) and exposed to liquid nitrogen source to maintain the crystal environment close to 100 K.[14] The single crystal X-ray diffraction data were collected in a full circle. Data reduction was performed using a Bruker SAINT software. Intensities for absorption were corrected using SADABS. The crystal structure was solved by direct methods, and SHELXS97[15] and OLEX 2.0 (ref. 16) were utilized for structure solution and least-squares refinement. The non-hydrogen atoms were refined anisotropically. Single crystal X-ray diffraction data, data collection and structure refinement details are summarized in Table 1. The C–H atoms were fixed at idealized positions and refined with a riding-model approximation: C–H = 0.95–1.00 Å with Uiso(H) = 1.5 Ueq (C-methyl) and 1.2 Ueq (C) for other H atoms. The N–H and O–H hydrogens were located from the difference Fourier map and refined further. Anisole solvent was found to be highly disordered even at 100 K and SQUEEZE procedure (using PLATON)[17] was applied to obtain the most accurate geometry of the cocrystal. A check of the final CIF files (CCDC no. 2067490, 2067491†) using PLATON did not show any missed symmetry. Hydrogen bonding interactions were analysed and finally calculated using the HTAB instruction in SHELXL[18], see Table 2. Mercury 3.9 software was used to make molecular graphics of the cocrystals.[19]

Computational details and methods

All the monomers and dimers of the complexes were optimized using DFT-B3LYP with 6-311++G** basis set.[20a] Optimized

Table 1 Crystallographic details for the MET cocrystals

	MET–SAM[a] (1 : 1)	MET–NAM (1 : 1)	MET–HBA[b] anisole hemisolvate (1 : 1 : 0.5)	MET–HBA anisole hemisolvate (1 : 1 : 0.5) after 3 months
CCDC no.	1841404	2067490	2067491	—
Chemical formula	$C_{12}H_{15}NO_3$, $C_7H_7NO_2$	$C_{12}H_{15}NO_3$, $C_6H_6N_2O$	$C_{12}H_{15}NO_3$, $C_7H_6O_3$, 0.5 (C_7H_8O)	$C_{12}H_{15}NO_3$, $C_7H_6O_3$, 0.5 (C_7H_8O)
M_r	358.39	343.38	413.44	413.44
Crystal system, space group	Triclinic, $P\bar{1}$	Triclinic, $P\bar{1}$	Triclinic, $P\bar{1}$	Triclinic, $P\bar{1}$
T (K)	298(2)	295(2)	100(2)	298(2)
a (Å)	5.2373(5)	5.4865(7)	5.1182(2)	5.1469(7)
b (Å)	10.9485(11),	10.4664(12)	13.3984(5)	13.5126(15)
c (Å)	15.5370(16)	15.4477(15)	14.4561(6)	14.6711(17)
α, β, γ (°)	83.000(6), 88.982(6), 81.834(6)	96.842(15), 90.303(11), 97.911(14)	89.4000(10), 88.7370(10), 89.3480(10)	88.316(3), 87.943(4), 88.945(3)
V (Å^3)	875.29(15)	872.16(17)	990.98(7)	1019.1(2)
Z	2	2	2	2
ρ_{calc} (g cm^{-3})	1.326	1.308	1.204	1.171
μ (mm^{-1})	0.099	0.772	0.090	0.088
Radiation	Mo Kα	Cu Kα	Mo Kα	Mo Kα
Specimen shape, size (mm)	0.24 × 0.20 × 0.20	Flat sheet, 15 × 1	0.30 × 0.20 × 0.16	0.30 × 0.20 × 0.16
Data collection no. of measured, independent and observed reflections	9342, 4010, 3442	—	32063, 6043, 5599	12037, 4388, 1924
θ values (°)	$\theta_{max} = 26.38$, $\theta_{min} = 2.56$,	$2\theta_{min} = 4.0$, $2\theta_{max} = 80.0$, $2\theta_{step} = 0.01$	$\theta_{max} = 30.5$, $\theta_{min} = 2.82$	$\theta_{max} = 30.2$, $\theta_{min} = 2.93$
Refinement R factors, wR_2, goodness of fit	0.0465, 0.1177, 1.045	$R_p = 0.0311$, $R_{wp} = 0.0408$, $R_{exp} = 0.0198$, $\chi 2 = 2.061$	0.0539, 0.1733, 1.070	0.1895, 0.5647, 1.780
Method of structure determination	SCXRD	PXRD	SCXRD	SCXRD

[a] Note: lattice parameters of MET–SAM was reported by us in ref. 8a. [b] In the refinement, scattering from the highly disordered anisole molecule was taken into account with the "SQUEEZE" procedure.

Open Access Article. Published on 15 September 2021. Downloaded on 4/7/2026 1:42:27 PM.
This article is licensed under a Creative Commons Attribution-NonCommercial 3.0 Unported Licence.

Table 2 Normalized hydrogen bond parameters[a]

Cocrystals	Hydrogen bonds	D–H Å^{-1}	D–H···A Å^{-1}	< D–H···A/°	Symmetry codes
MET–NAM	N1–H1···O3	2.29	3.0707(4)	151	$-x, 2-y, 1-z$
	N2–H2A···O4	2.11	2.9670(4)	179	$3-x, 1-y, 1-z$
	N2–H2B···O3	2.20	3.0318(4)	161	$1+x, y, z$

[a] Note: H bond parameters of MET–HBA (anisole) solvate are not summarized due to disordered solvent.

geometries were used to study the strength of both homo and hetero dimers at same level of theory. In addition, vibrational harmonic frequency calculation was carried out to ensure the minimum energy conformations of the all clusters. The binding energy (BE) of the complexes are calculated using the supramolecular approach and corrected for basis set superposition error (BSSE) employing the counterpoise (CP) procedure suggested by Boys and Bernardi[20b] in eqn (1),

$$\mathrm{BE} = -\left(E_{\mathrm{complex}} - \sum_{i=1}^{n} E_{\mathrm{i}}\right) \quad (1)$$

where, E_{complex} is the total energy of the dimer, E_{i} is energy of the monomer (*i.e.* MET, NAM, HBA). In order to quantify the role of dispersion energy of these dimers, dispersion correction term BEs (DFT-D3) was also included.[20c] All the electronic structure calculations were performed using *GAUSSIAN 16* and Chemcraft software's were used for visualization.[20d]

Powder dissolution

In order to access dissolution profile of MET cocrystals with NAM, SAM and HBA compared to the native drug, United State Pharmacopoeia (USP) dissolution apparatus II (paddle method) was employed on an Agilent 708-DS dissolution tester. Following sieving through standard mess sieves of 200 μm, metaxalone (200 mg) and its cocrystals (200 mg equivalent) added into the 500 ml pH 6.8 phosphate buffer medium at 37 °C. The dissolution experiment was continued till 16 h with the paddle rotation speed of 100 rpm, although saturation of solubility was observed within 4 h. The aqueous solution was collected at a definite time interval of 5, 10, 20, 30, 45, 60, 90, 120, 150, 180, 210, 240, 960 min and filtered through 0.45 μm nylon filter. Finally the absorbance's of the solution was measured at 217 nm using UV-Vis spectrophotometer to avoid interference from the coformers (λ_{NAM} = 260 nm, λ_{SAM} = 300 nm, λ_{HBA} = 254 nm). The absorption coefficients of MET and its cocrystals were determined from the slope of absorbances of known concentration. Final concentration of the drug was calculated using Lambert–Beer's law.

Results and discussion

Absence of ionizable group in the drug assure the possibility of cocrystals during multicomponent solid form screening. MET is reported to form cocrystals with SAM, NAM and HBA.[8a] In this communication, the cocrystal structures of MET–NAM (1 : 1) and MET–HBA (1 : 1) with 0.5 eq. of anisole solvate are discussed including isostructurility with the reported MET–SAM cocrystal, followed by their solubility improvement.

MET–NAM (1 : 1) cocrystal

The crystal structure was solved in triclinic $P\bar{1}$ space group with one molecule each of MET and NAM in the asymmetric unit. Similar to reported MET cocrystals with carboxylic acids and amides,[7a,8a] both the drug and NAM form N–H···O hydrogen bonded imide–imide (N1–H1···O3: 2.29, 3.07 Å, 150.8°) and amide–amide (N2–H2A···O4: 2.11, 2.96 Å, 179.4°) centrosymmetric hydrogen bonded homodimers of $R_2^2(8)$ ring. The hydrogen bonding parameters indicate the stronger hydrogen bonded NAM dimer than the MET imide dimer. These two homodimers are integrated by the *anti*-NH group of NAM, which constitute intermolecular N–H···O hydrogen bond (N2–H2B···O3: 2.20, 3.03 Å, 161.4°) with the bifurcated carbonyl group of the drug that is extended parallel to the *b*-axis, see Fig. 2a. The tetramer containing phenyl rings of the drug molecules and NAM dimer are placed in an acute angle of 56.5°. Surprisingly, pyridine nitrogen atom of NAM does not involve in any kind of hydrogen bonding neither with the drug nor the coformer, similar to reported lesinurad–nicotinamide cocrystal.[13c] In addition, C–H···π interactions (between phenyl CH of drug and aromatic ring of NAM) further stabilizes the cocrystal assembly *via* tetramer formation; see Fig. 2b. 3D packing viewed down the crystallographic *a* axis indicates similar to a host–guest assembly, wherein NAM dimer (orange circle) is surrounded by MET hexamer; see Fig. 2c, which is identical to the reported MET–SAM (1 : 1) cocrystal[8a] (Fig. S2, ESI†).

MET–HBA cocrystal (anisole hemisolvate)

Harvesting good quality single crystals of MET–HBA cocrystal from methanol or acetone afforded nonstoichiometric hydrate of the binary system, for which we could not able to harvest suitable single crystals.[8a] Rather, suitable needle crystals were obtained from anisole solvent *via* slow evaporation. The corresponding crystal structure was solved in triclinic $P\bar{1}$ space group and the asymmetric unit contains one molecule each of MET and HBA along with half equivalent anisole solvent in highly disordered state even at 100 K. Following removal of the disordered (anisole) fragments using SQUEEZE, the cocrystal packing exhibits voids with the volume of 120 Å^3, where no more than 8 atoms can fit (15 Å^3 per atom), that suggests a possibility of anisole molecule, not water in the crystal lattice. Therefore, the stoichiometry of the cocrystal is MET : HBA : anisole = 1 : 1 : 0.5. Following SQUEEZE procedure, the

 © 2021 The Author(s). Published by the Royal Society of Chemistry

Open Access Article. Published on 15 September 2021. Downloaded on 4/7/2026 1:42:27 PM.
This article is licensed under a Creative Commons Attribution-NonCommercial 3.0 Unported Licence.

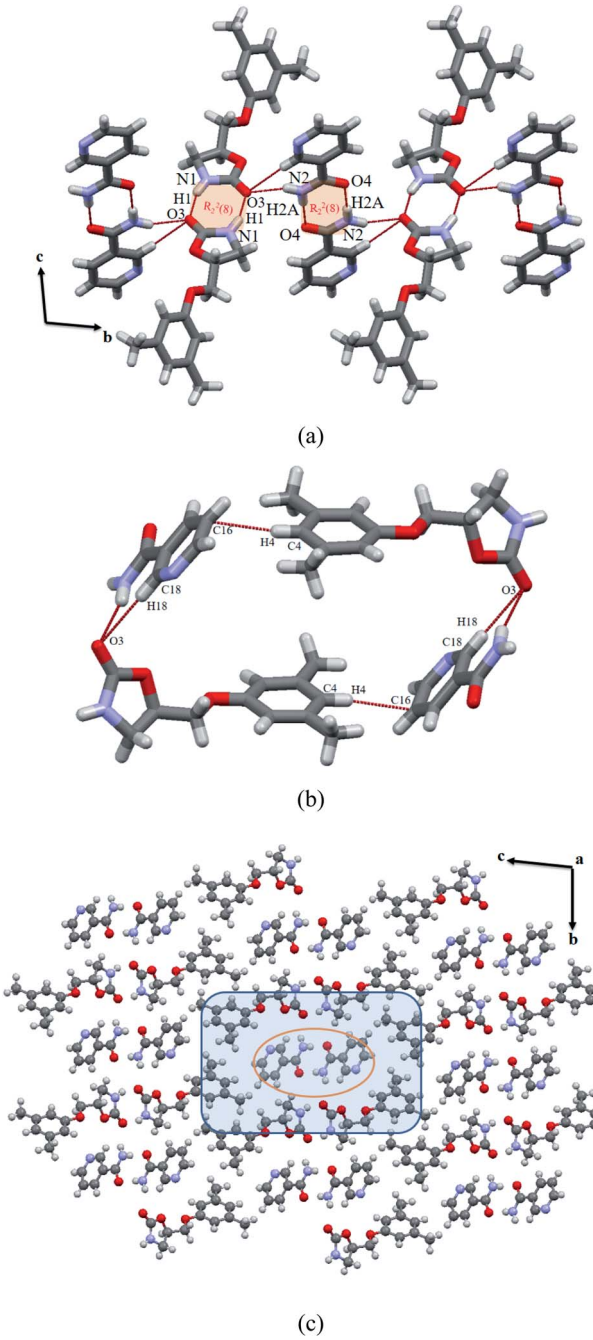

Fig. 2 (a) Hydrogen bonded MET–NAM (1 : 1) cocrystal, wherein two homosynthons are bound by intermolecular N–H···O interactions. (b) Auxiliary C–H···O/π interactions between MET and NAM to form tetramer motif. (c) Host (MET)–guest (NAM) assembly of the cocrystal.

most accurate geometry of the cocrystal was obtained with crystal void dedicated for anisole molecule.[21] The cocrystal structure consists of drug–drug and acid–acid homosynthons of $R_2^2(8)$ ring *via* hydrogen bonded imide–imide (N1–H1···O1: 1.99, 2.85 Å, 160.5°) and acid–acid (O6–H61···O4: 1.67, 2.62 Å, 166.6°) centrosymmetric dimers; see Fig. 3a. The hydrogen bond distances suggest that stronger imide homodimer in the drug is observed here than in the MET–NAM cocrystal. These

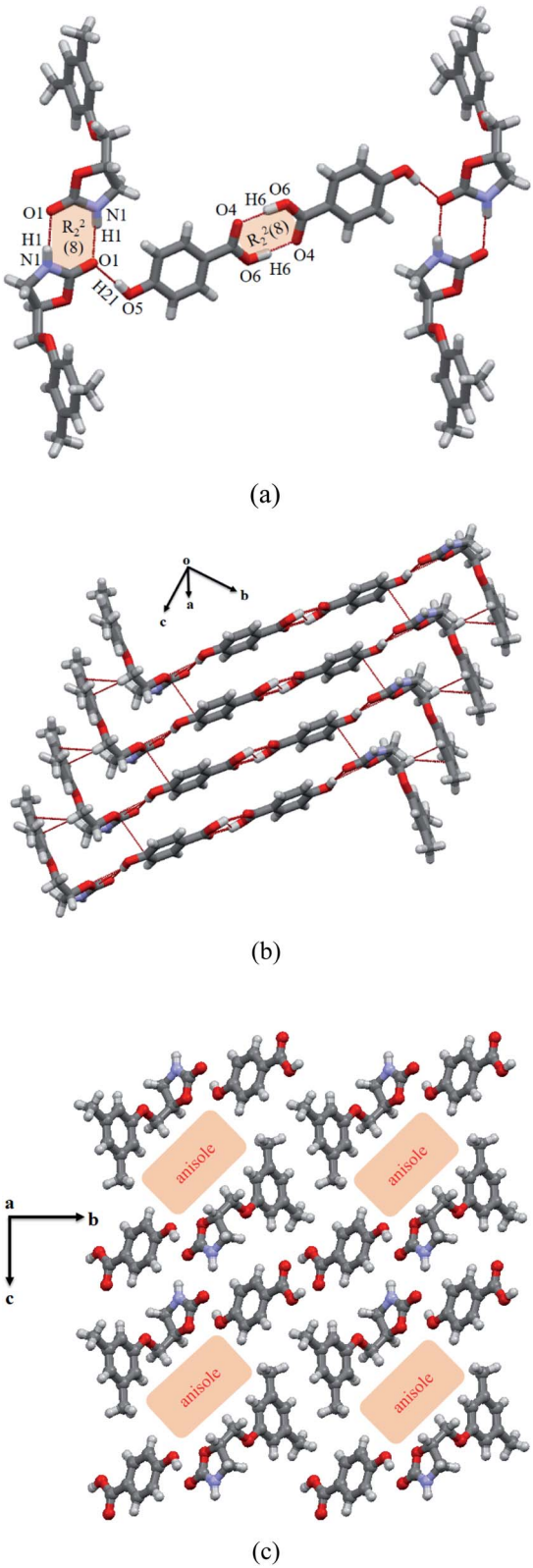

Fig. 3 (a) Hydrogen bonded MET–HBA cocrystal (anisole hemisolvate) wherein two individual homodimers are bound by intermolecular O–H···O interactions. (b) Stacking between the tetramer units of MET and HBA. (c) 3D packing view of the anisole solvate down the *a* axis.

Open Access Article. Published on 15 September 2021. Downloaded on 4/7/2026 1:42:27 PM.
This article is licensed under a Creative Commons Attribution-NonCommercial 3.0 Unported Licence.

two homodimers are interlinked by the hydroxyl group of HBA, which constitutes intermolecular O–H···O hydrogen bond (O5–H21···O1: 1.87, 2.67 Å, 172.9°) with the bifurcated carbonyl group of the MET and extended diagonal to the *ab*-plane. The phenyl ring containing planes of the drug and HBA homodimers are arranged in an almost perpendicular fashion (84.4°). A stepwise layer structure is formed by off-stacked (cg:cg = 4.36 Å) between benzene ring of HBA and oxazolidinone ring of the drug. In addition, C–H···π stacking interactions (H:cg = 2.56 Å) between two MET molecules are observed in between the layers; see Fig. 3b. A clear void of anisole solvate exists when viewed the 3D packing down the crystallographic *a* axis (Fig. 3c). The single crystal (of cocrystal solvate) was found to be stable in a glass vial for more than three months at ambient conditions as evidenced by its identical lattice parameters, see Table 1. This indicates that the oxygen atom of the anisole may involve in several auxiliary interactions with the drug or coformers that renders it's excellent stability. Possibility of partial hydrate formation might be ruled out by examining the volume of the void as both are quite close and little differences (991 and 1019 $Å^3$) are observed due to temperature variation.

Isostructurility of MET–NAM/SAM cocrystals

The 2D/3D isostructural multicomponent solids like cocrystals, salts, solvates with the exchange of functional groups or elements like CH_3/Cl, CH/N, NH/OH, Cl/Br are well-known in the literature.[22] Lattice parameters of MET–NAM and MET–SAM cocrystals are similar that suggest their isostructural packing, see lattice parameters in Table 1. Hydrogen bonded motifs involving imide–imide (drug) and amide–amide (coformer) homosynthons and their 3D view of both MET–NAM and MET–SAM cocrystals retain similarity; see Fig. 2 and S2, ESI.† Their unit cell similarity index ($\Pi = 0.0102$) is very close to zero that indicates the two units cells exist in similar shape and volume.[23]

Using XPac software,[24] cocrystal structural comparison was carried out by introducing a coordination sphere of 14 molecules around a central molecule using symmetric operations related to the space group ($P\bar{1}$) of both the crystal structures. Based on the angular (a), planar (p) and distance (d) relationships, a total of 196 parameters were introduced between the central kernel molecule and a surrounding molecule in the cluster. Xpac analysis of the two cocrystals suggests the nearer placement of the (δa, δp) points to the origin of the system, which further confirm their isostructurility, see Fig. S3, ESI.† Similarity of these sets of parameters connects in the position of molecules in the cluster and finally dimensionality of the similarity was derived. In these two cocrystals, 10 MET molecules were matched out of 14 nearest neighbours in the cluster that suggests layer of molecule similarity. The corresponding dissimilarity index ($X = 5.6$) suggests a supramolecular construct with 2D isostructurility (Fig. 4a). The amide coformers such as NAM and SAM are structure wise very similar except additional *ortho* hydroxyl group in the latter, which takes part in an intramolecular hydrogen bonding with the amide carbonyl. The molecular overlay of the drug conformers in MET–NAM and MET–SAM cocrystal pair further support their isostructurility, see Fig. 4b Hence, it was

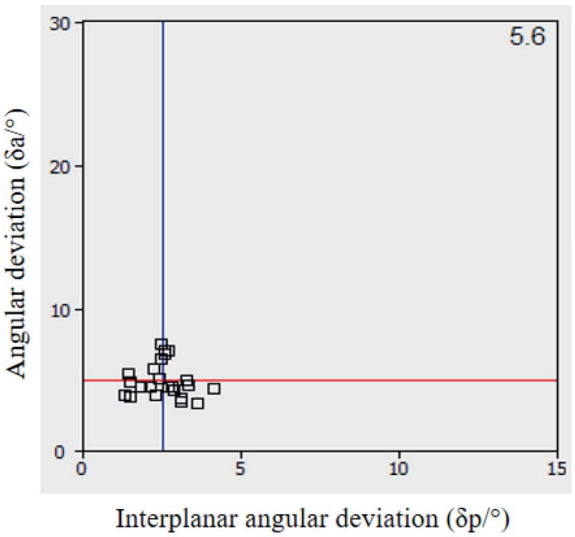

(a)

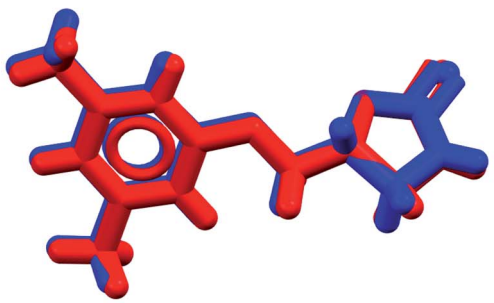

(b)

Fig. 4 (a) XPac plot of interplanar angular deviation (δp/°, *x* axis) *vs.* angular deviation (δ*a*/°, *y* axis) of the MET–NAM and MET–SAM cocrystal pair illustrating their 2D structural similarity with layers of molecules match. (b) Molecular overlay diagram of MET in MET–SAM (red) and MET–NAM (blue trace) reinforces their isostructurility.

expected that the corresponding cocrystals may display isostructurility. On the other hand, HBA is quite different from the amide coformers in terms of functional groups and their orientations that resulted different structural cocrystal.

Molecular conformations

Metaxalone crystallized as Form A ($Z' = 2$, two symmetry independent molecules) and Form B ($Z' = 1$), in which oxazolidinone ring is highly flexible compared to the planar 3,5-dimethylphenoxymethyl fragment.[6a] In fact, one of the conformation of Form A (II) is very similar to that of Form B. The orientation of the five membered cyclic ring compared to the aryl moiety that confirms slight change of torsion along the C–C bond connecting those two terminal rings. This results several conformations of MET, which are observed in its polymorphs and cocrystals[7a,8a] (Fig. 5). The molecular conformations of MET in MET–NAM and MET–SAM cocrystals are identical, see Fig. 4b. Conformational differences are quantitatively measured by the dihedral angle between two planes containing aryl and oxazolidinone rings that

© 2021 The Author(s). Published by the Royal Society of Chemistry

Open Access Article. Published on 15 September 2021. Downloaded on 4/7/2026 1:42:27 PM.
This article is licensed under a Creative Commons Attribution-NonCommercial 3.0 Unported Licence.

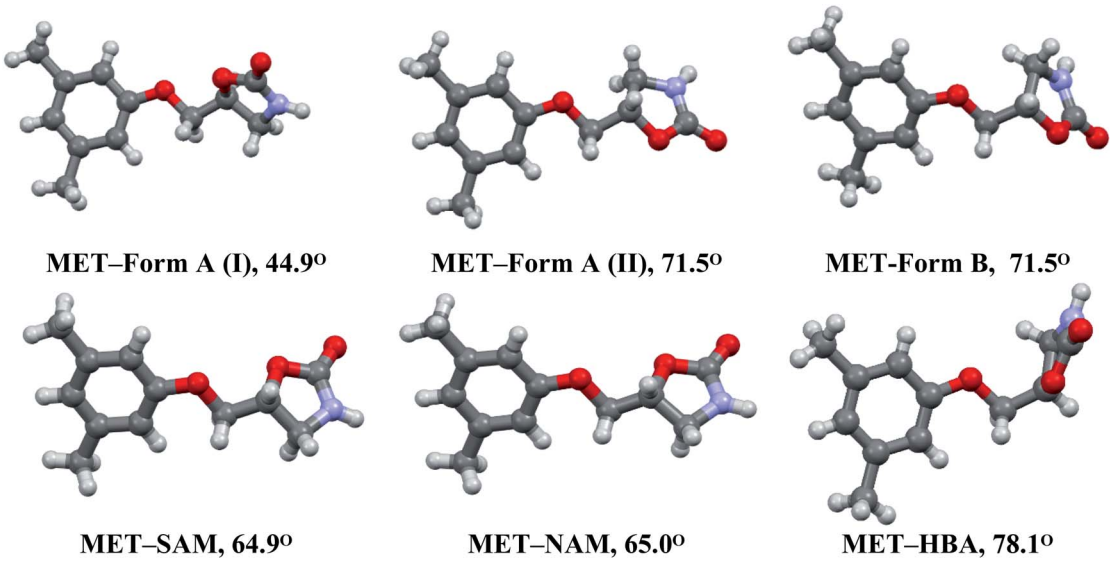

Fig. 5 The molecular conformations of MET in its polymorphs and cocrystals. The dihedral angles (°) are originated by the planes of aryl and oxazolidinone rings.

confirms the similar MET conformation in MET–NAM and MET–SAM cocrystals, which extends support of their isostructurility. Among the six MET conformations, the drug with close to perpendicular arrangement between the planes of aryl and oxazolidinone rings is observed in MET–HBA (anisole) cocrystal. The molecular conformation of the drug is very important as it may have direct impact on the solubility behaviour of the cocrystals (discussed at the end).

Binding energy and stability

The optimized geometries of all the homo and hetero-synthon (*i.e.* MET, NAM and HBA) complexes are shown in Fig. 6. The calculated hydrogen bonding (H-bonding) distances (in Å) along with the respective BEs of the clusters (in kcal mol^{-1}) are provided. BE reveals that HBA dimer (II) complex is more stable than the other homo dimers (*i.e.* MET and NAM). The enhanced stability arises from the formation of perfect donor–acceptor H-Bond pattern in HBA (carboxylic acid) dimer. The existence of shorter O–H···O H-bonding (~1.66 Å) in HBA dimer (II) may enhance the stability of the complexes. Although, other MET and NAM homodimers form imide/amide H-bonds with the much longer distance of ~1.87 to 2.27 Å. This is significantly longer than the HBA dimer (II) complex. Hence, the stability order of homo dimers is HBA (II) > MET > NAM (II). It is found from our study, other possible less stable dimers of the coformers also exist with comparatively lower BE. But, the mode of interactions of these clusters are not observed exactly in the crystal packing. During incorporation of MET in these clusters, the energetics of the complexes varies from ~17.5 to 19.5 kcal mol^{-1}. The calculated BE value reveal that MET homodimer (~17.9 kcal mol^{-1}) is slightly more stable than MET–NAM (~17.5 kcal mol^{-1}) and at the same time, MET–HBA complex (~19.5 kcal mol^{-1}) is more stable than the other complexes. The interaction strength of H-bonded MET–HBA dimer energy is ~1.6 kcal mol^{-1} higher than the respective MET homodimer. It is interesting to note that, the less stable MET–HBA (I) isomer is very relevant to the experimental crystal structure, which is stabilized by O–H···O H-bonded intermolecular interaction between HBA (OH) and MET (C=O) functional group (Fig. 3a). The calculated H-bond distance (~1.82 Å) confirms the strength of hydrogen bond. Even though, this mode of interaction in MET–HBA (I) is less stable, the molecular arrangement of MET–HBA cocrystal structure confirms that this is the most favourable cluster along with the individual homodimers. The carboxylic acid dimer is more favourable mode of interaction in the MET–HBA (II) complex. In the cocrystal structure, HBA dimer (II) acts as a bridge between two MET homodimers. The BE calculations of the MET–NAM/HBA heterodimers confirm that along with the MET homodimer, MET–coformer heterodimers are also possible specially in case of MET–HBA cocrystal. In case of MET–SAM and MET–NAM (II) complexes, the corresponding BEs are 1.0 and 0.4 kcal mol^{-1} lower than the MET homodimers that support their experimental cocrystal structures with the individual homodimers, see Fig. 2a and S1a.† The higher BE of MET–HBA (II) heterodimer than MET homodimer suggests the possibility of heterosynthon which can be obtained experimentally. In fact, we suggested the possibility of imide (MET)···acid (HBA) heterodimers in MET–HBA (hydrate) based on its vibrational frequency data, for which we could not able to get the cocrystal structure.[8a]

Powder X-ray diffraction

X-ray diffraction is a non-destructive method to characterize a solid form as every compound has its own characteristic finger print region of X-ray patterns. The technique is mainly used for phase identification of a crystalline phase like polymorph, cocrystals, salts *etc.* During cocrystal screening, changes in XRD pattern compared to the native drug and coformer confirm the possibility of new solid form. The crystal structure of MET–NAM was obtained from high resolution XRD data of which Rietveld plot is displayed in Fig. S1, ESI.† On the other hand, XRD

Open Access Article. Published on 15 September 2021. Downloaded on 4/7/2026 1:42:27 PM.
This article is licensed under a Creative Commons Attribution-NonCommercial 3.0 Unported Licence.

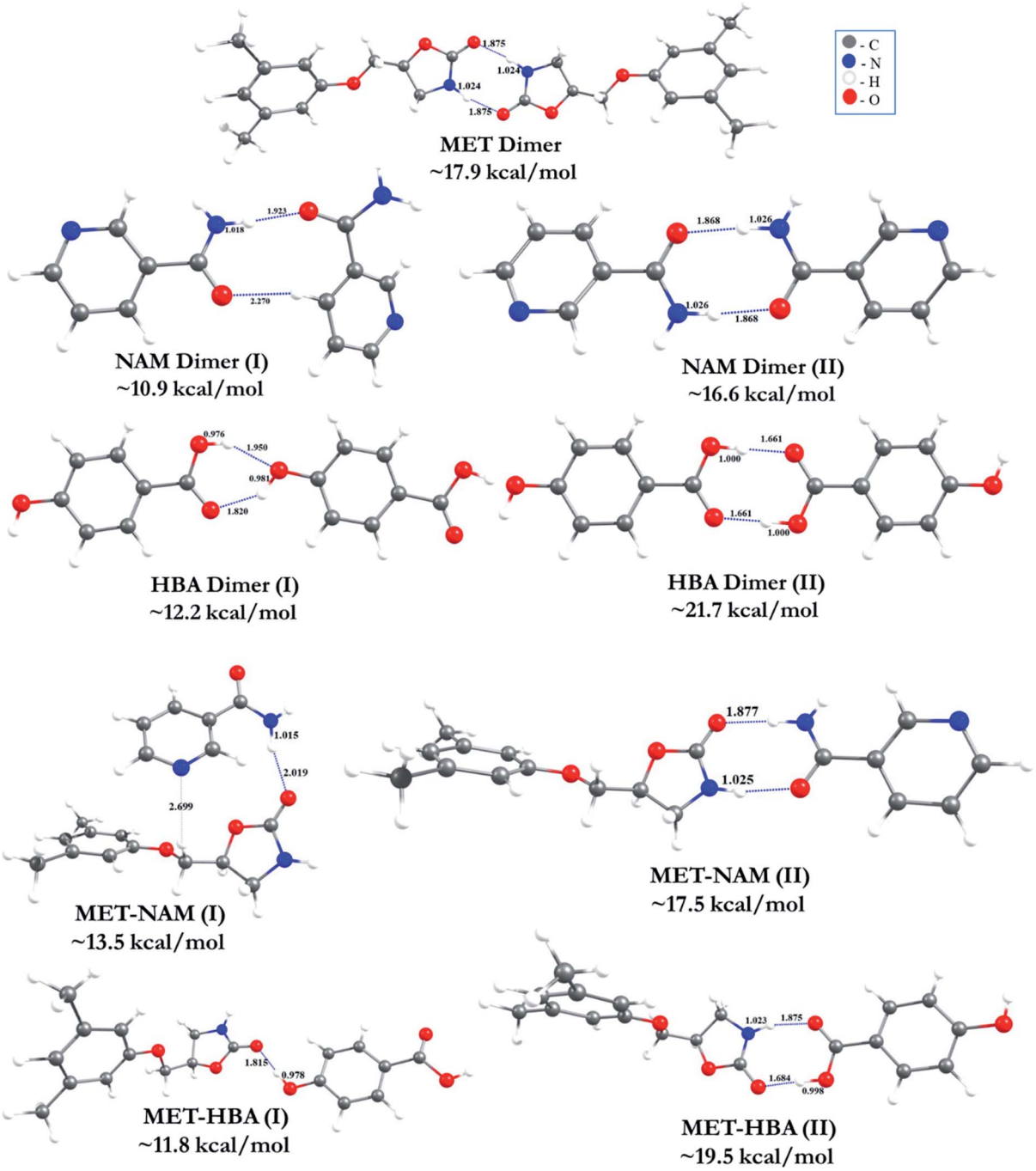

Fig. 6 DFT optimized geometries and calculated BEs of homo and heterodimers (distances and BEs are in Å and kcal mol^{-1}, respectively).

pattern of MET–HBA cocrystal obtained from slurry in anisole broadly matches with its cocrystal structure that may be due to the temperature difference between single crystal (100 K) and powder X-ray diffraction data (298 K) collection and also possibility of partial solvent (anisole) loss from the powdered cocrystal at ambient conditions.

Thermal analysis

The novel binary solid form can be additionally characterized by its distinguished melting endotherm that needs to be different from either that of the drug or coformer. All the MET–NAM/SAM/HBA cocrystals exhibited lower melting endotherms compared to the native drug and coformer, which is common among 29% of the reported cocrystals.[8a,25] Commercial MET Form A (black trace) exhibited single melting endotherm peak at 126.2 °C, whereas MET–NAM (red trace), MET–SAM (blue trace) melted at 107.4 and 119.5 °C respectively. Surprisingly, both MET–NAM and MET–SAM showed similar enthalpy of fusion (125.7; 126.4 J g^{-1}) and entropy of fusion (0.33; 0.32 J g^{-1} K^{-1}) that further support their isostructural packing. MET–HBA 0.3 hydrate (magenta trace) exhibited 1st endotherm at 104.4 °C (due to dehydration), followed by melting endotherm at

© 2021 The Author(s). Published by the Royal Society of Chemistry

Open Access Article. Published on 15 September 2021. Downloaded on 4/7/2026 1:42:27 PM.
This article is licensed under a Creative Commons Attribution-NonCommercial 3.0 Unported Licence.

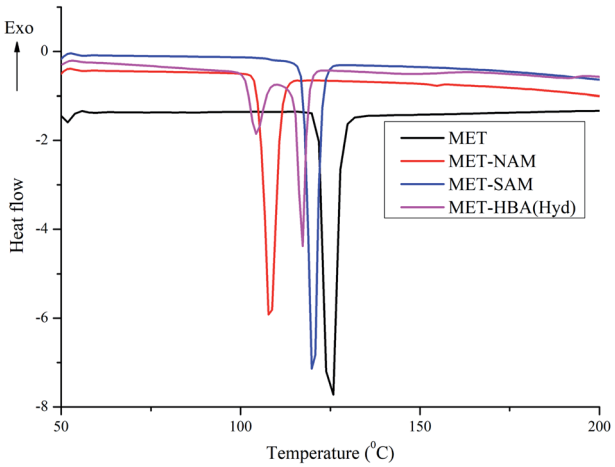

(a)

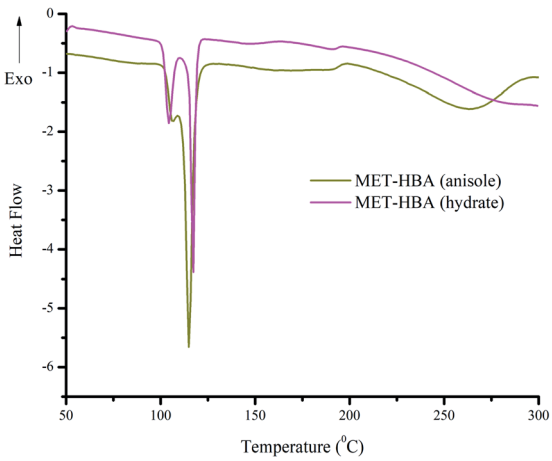

(b)

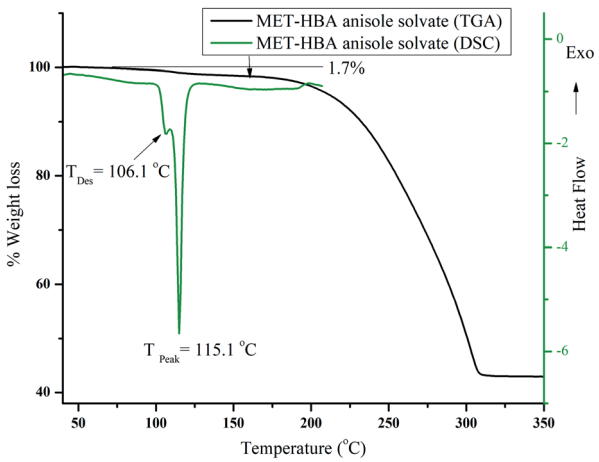

(c)

Fig. 7 DSC endotherms of (a) MET (Form A) and its cocrystals, (b) MET–HBA (hydrate) and MET–HBA (anisole). (c) DSC and TGA comparison of MET–HBA (anisole).

116.5 °C, see Fig. 7a. Interestingly, MET–HBA (anisole solvate, dark yellow trace) showed a minor endotherm at 106.1 °C, followed by sharp melting at 115.1 °C. Desolvation of anisole (bp 154 °C) at ~106 °C confirms its weak interactions with the drug/coformer. In addition, both the MET–HBA cocrystal hydrate/anisole solvate melted at similar temperature after water/solvent loss, see Fig. 7b. Thermogravimetric analysis (TGA) of MET–HBA cocrystal (anisole solvate) indicated only 1.7% weight loss, which is much lower than the calculated one (11.5%) corresponds to 0.5 equivalent of anisole (Fig. 7c). TGA data suggests only 0.07 equivalent of anisole is present in the crystal lattice of MET–HBA cocrystal that is much lower than its cocrystal structure with the suggested 0.5 equivalent of anisole. This indicates loosely bound anisole with the host (cocrystal) and the possibility of partial solvent loss from the cavity of the cocrystal at ambient conditions. It is anticipated that the a small fraction of the anisole solvent slowly disappeared from the cocrystal lattice during three months storage at ambient conditions that was confirmed by the small desolvation endotherm at 100.8 °C, followed by melting endotherm (117.8 °C) in a DSC of the corresponding single crystals. Although, the same crystals exhibited little lower weight loss of 1.4% in a TGA analysis, see Fig. S4, ESI.† Lower melting endotherms of MET cocrystals are supposed to improve the solubility/dissolution profile of the native drug.[26]

Dissolution experiment

Solubility of a solid form depends upon particle size, morphology, lattice energy, solvation energy, pH and temperature of the medium. MET is a poor aqueous soluble drug due to presence of hydrophobic aromatic skeleton and cyclic carboxamate ring. Improving solubility of MET is an utmost important in order to enhance its bioavailability and also decrease the toxic side effect. Powder dissolution of MET and its cocrystals including MET–HBA (hydrate) in pH 6.8 phosphate buffer medium suggests that MET–NAM cocrystal enhanced the aqueous solubility (8.6 fold) of the native drug within 4 h,

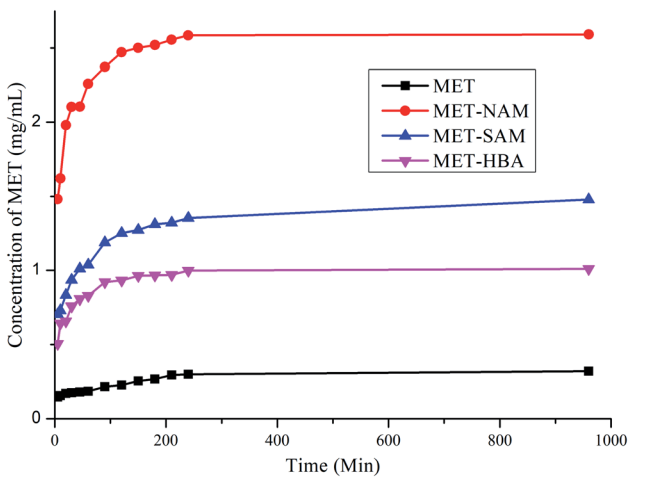

Fig. 8 Powder dissolution of MET and its cocrystals in pH 6.8 phosphate buffer at 37 °C.

Open Access Article. Published on 15 September 2021. Downloaded on 4/7/2026 1:42:27 PM.
This article is licensed under a Creative Commons Attribution-NonCommercial 3.0 Unported Licence.

Table 3 Solubility of MET and its cocrystals in pH 6.8 phosphate buffer at 37 °C

API/cocrystals	Apparent solubility (mg ml^{-1}) at 4 h	Aqueous solubility (g L^{-1}) of the coformers	mp (T_{peak}/°C) of the drug/cocrystals	Nature of the powder samples during dissolution	Solid phase transformation after dissolution experiment
MET (Form A)	0.30	—	126.2	Sticky	MET (Form A)
MET–NAM	2.58 (×8.6)	500	107.4	Initially sticky for short time, followed by free flow	MET (Form A)
MET–SAM	1.35 (×4.5)	2.1	119.5	Initially sticky, followed by free flow	MET–SAM + MET (Form A)
MET–HBA (hydrate)	1.01 (×3.4)	5.0	116.5	Free flow	MET–HBA + MET (Form A)

followed by MET–SAM and MET–HBA (hydrate), see Fig. 8. Apparent solubility of the cocrystals are summarized in Table 3. As expected, MET cocrystals exhibited higher aqueous solubility than the native drug due to presence of high soluble coformers. Except, MET–SAM cocrystals, others got saturation in solubility within 4 h of the dissolution experiment. Higher solubility of the cocrystals can be explained based on the solubility and melting point of the coformer, see Table 3. Higher solubility of NAM and lower melting point of MET–NAM played an important role in enhancing aqueous solubility of the native drug. More solubility of HBA than SAM and slightly lower melting point of the corresponding cocrystal did not guarantee higher solubility of the drug due to presence of 0.3 equivalent water molecule in the crystal lattice of MET–HBA. Hydrates are generally less soluble than their anhydrous counterparts due to higher lattice energy.[27] In addition, all the cocrystals melted lower than the native drug that qualify the thumb rule of inverse correlation between solubility and melting point.[26] Hence the aqueous solubility order is justified as MET–NAM > MET–SAM > MET–HBA (hydrate)> MET.

Based on the structural point of view, N–H···O (D···A) bond distances of MET polymorphs and cocrystals decrease in the order of Form A (2.84 Å, 160.4°), MET–HBA (2.85 Å, 160.5°), Form B (2.87 Å, 161.3°), MET–SAM (2.89 Å, 168.0°) and MET–NAM (3.03 Å, 161.5°). This data indicates that MET dimer becomes much weaker in MET–NAM cocrystal than MET–HBA and Form A; whereas MET–SAM has intermediate bond strength. In addition, intermolecular N–H···O hydrogen bonding between the drug and coformer becomes weaker in MET–NAM (3.03 Å, 161.5°) than MET–SAM (2.99 Å, 166.3°). In MET–HBA cocrystal, intermolecular O–H···O hydrogen bonding between MET and HBA is equally strong (2.67 Å, 172.9°) compared to HBA dimer (2.62 Å, 166.6°). These structural features indicate that MET–NAM is easy to dissociate compared to other two cocrystals during dissolution experiment that helps the drug to obtain its high energy metastable phases *via* parachute effect[28] and enhance the solubility of the bioactive substance.

Following powder dissolution experiment after 16 h, the residues were characterized by XRD to confirm whether cocrystals retained or transformed to the native drug. According to US-FDA guidelines (2013, 2018), the pharmaceutical cocrystals need to dissociate before reaching the target site of biological action. MET–NAM cocrystal completely transformed to MET (Form A), whereas MET–SAM/HBA cocrystals partially converted to the native drug, see Fig. S5, ESI.† This may be explained due to much higher solubility of NAM compared to the native drug, which forms a non-congruent system that dissociated much faster.[29] Comparatively, SAM and HBA are low aqueous soluble coformers that form congruent binary system with the drug and hence partially dissociated over the time period. Although MET–HBA (hydrate) was free flow in nature throughout the dissolution experiment, but not suitable because of its lower solubility. On the other hand, MET–NAM cocrystals were initially sticky for a shorter time, followed by free flow during dissolution experiment. To summarize, MET–NAM cocrystal may be promising solid form in improving bioavailability of the drug and decreasing its side effects.

Conclusions

Metaxalone, a muscle relaxant and pain killer drug exhibits poor aqueous solubility and bioavailability due to absence of polar functional groups. The drug was cocrystallized with NAM and HBA in order to improve its aqueous solubility. MET cocrystal with NAM is an anhydrous one, whereas with HBA it crystallized as either hydrate or anisole solvate. Both the cocrystals maintain the presence of imide···imide (drug) and amide···amide/acid···acid (coformer) homosynthons, that is similar to the reported ones. Lower binding energy of MET heterodimer supports the preference of the drug homodimer in the cocrystals. MET cocrystals with NAM and SAM exhibit 2D isostructural packing confirmed by unit cell similarity index, and dissimilarity index (XPac analysis). Even similar enthalpy and entropy of fusion of the cocrystals support their isostructurility. Dissolution experiments of MET cocrystals indicated the superior solubility of MET–NAM than other cocrystals and the native drug that was correlated based on its lower melting point, higher solubility of NAM and weaker intermolecular interaction between MET and NAM. In addition, MET–NAM cocrystal dissociated and transformed to MET (Form A) during dissolution experiment, which offer advantage of higher solubility. Improved solubility of MET–NAM is anticipated to enhance the drug's bioavailability and decrease side effect.

Conflicts of interest

There are no conflicts to declare.

© 2021 The Author(s). Published by the Royal Society of Chemistry

Open Access Article. Published on 15 September 2021. Downloaded on 4/7/2026 1:42:27 PM.
This article is licensed under a Creative Commons Attribution-NonCommercial 3.0 Unported Licence.

Acknowledgements

We acknowledge Dr V. A. Tafeenko for the valuable advices in disorder modeling for MET–HBA (anisole) structure. S. K. G. thanks Lupin Ltd. for providing research facilities to carry out the research work as a part of PhD Ascent program. P. S., V. P. and M. P. thank SRM Institute of Science and Technology for giving basic research facilities and acknowledge DST-FIST fund (No. SR/FST/CST-266/2015(c)) for improvement of S&T infrastructures of Department of Chemistry. The authors also thank SRM-IST for providing the supercomputing facility.

References

1 (*a*) G. Bolla and A. Nangia, *Chem. Commun.*, 2016, **52**, 8342–8360; (*b*) N. K. Duggirala, M. L. Perry, O. Almarsson and M. J. Zaworotko, *Chem. Commun.*, 2016, **52**, 640–655; (*c*) M. Karimi-Jafari, L. Padrela, G. M. Walker and D. M. Croker, *Cryst. Growth Des.*, 2018, **18**, 6370–6387; (*d*) O. N. Kavanagh, D. M. Croker, G. M. Walker and M. J. Zaworotko, *Drug Discovery Today*, 2019, **24**, 796–804.

2 US-FDA, *Regulatory Classification of Pharmaceutical Co-Crystals Guidance for Industry*, 2018, https://www.regulations.gov/document/FDA-2011-D-0800-0029.

3 (*a*) G. Bolla, P. Sanphui and A. Nangia, *Cryst. Growth Des.*, 2013, **13**, 1988–2003; (*b*) A. Gunnam, K. Suresh, R. Ganduri and A. Nangia, *Chem. Commun.*, 2016, **52**, 12610–12613.

4 (*a*) G. Portalone, *Crystals*, 2020, **10**, 999–1012; (*b*) M. K. Dudek, E. Wielgus, P. Paluch, J. Śniechowska, M. Kostrzewa, G. M. Day, G. D. Bujacz and M. J. Potrzebowski, *Acta Crystallogr., Sect. B: Struct. Sci., Cryst. Eng. Mater.*, 2019, **B75**, 803–814; (*c*) F. Y. Wang, Q. Zhang, Z. Zhang, X. Gong, J. R. Wang and X. Mei, *CrystEngComm*, 2018, **20**, 5945–5948; (*d*) B. Swapna, D. Maddileti and A. Nangia, *Cryst. Growth Des.*, 2014, **14**, 5991–6005.

5 (*a*) R. B. Bruce, L. Turnbull, J. Newman and J. Pitts, *J. Med. Chem.*, 1966, **9**, 286–288; (*b*) Metaxalone belongs to BCS Class II drug, see https://www.accessdata.fda.gov/drugsatfda_docs/nda/2015/022503Orig1s000ClinPharmR.pdf.

6 (*a*) S. Aitipamula, P. S. Chow and R. B. H. Tan, *Cryst. Growth Des.*, 2011, **11**, 4101–4109; (*b*) A. A. Bredikhin, D. V. Zakharychev, A. T. Gubaidullin and Z. A. Bredikhina, *Cryst. Growth Des.*, 2018, **18**, 6627–6639.

7 (*a*) J. Holland, C. Frampton, A. Chorlton and D. Gooding, *US pat.*, 8871793B2, 2010; (*b*) H. L. Lin, T. K. Wu and S. Y. Lin, *Thermochim. Acta*, 2014, **575**, 313–321.

8 (*a*) S. V. Gohel, P. Sanphui, G. P. Singh, K. Bhat and M. Prakash, *J. Mol. Struct.*, 2019, **1178**, 479–490; (*b*) M. S. Aziz, C. Gupta and L. K. Tyagi, *Indian J. Pharm. Sci.*, 2020, **82**, 974–983.

9 (*a*) D. A. Bender, *Nutritional Biochemistry of the Vitamins*. Cambridge University Press, 2003, p. 203; (*b*) *WHO Model Formulary*, ed. M. C. Stuart, M. Kouimtzi and S. R. Hill, World Health Organization, 2008, p. 496.

10 E. M. Bavin, F. J. Macrae, D. E. Seymour and P. D. Waterhouse, *J. Pharm. Pharmacol.*, 1952, **4**, 872–878.

11 (*a*) C. Vaisali, P. D. Belur and I. Regupathi, *LWT–Food Sci. Technol.*, 2016, **69**, 153–160; (*b*) US-FDA, *Nutrition, Center for Food Safety and Applied. "Ingredients - Parabens in Cosmetics"*, 2016, https://www.fda.gov/cosmetics/cosmetic-ingredients/parabens-cosmetics.

12 (*a*) C. Guo, Q. Zhang, B. Zhu, Z. Zhang, X. Ma, W. Dai, X. Gong, G. Ren and X. Mei, *Cryst. Growth Des.*, 2020, **20**, 3053–3063; (*b*) R. Thakuria and B. Sarma, *Crystals*, 2018, **8**, 101; (*c*) R. Thipparaboina, D. Kumar, R. B. Chavan and N. R. Shastri, *Drug Discovery Today*, 2016, **21**, 481–490.

13 (*a*) S. G. Zhukov, V. V. Chernyshev, E. V. Babaev, E. J. Sonneveld and H. Schenk, *Z. Kristallogr.*, 2001, **216**, 5–9; (*b*) V. B. Zlokazov and V. V. J. Chernyshev, *Appl. Crystallogr.*, 1992, **25**, 447–451; (*c*) V. Palanisamy, P. Sanphui, M. Prakash and V. Chernyshev, *Acta Crystallogr., Sect. C: Struct. Chem.*, 2019, **C75**, 1102–1117.

14 Bruker, *APEX 2 software for crystal structure data collection, refinement and structure solution*, Bruker AXS Inc., Madison, Wisconsin, 2006, https://www.brukersupport.com/ProductDetail/1148.

15 G. M. Sheldrick, *Acta Crystallogr., Sect. A: Found. Crystallogr.*, 2008, **A64**, 112–122.

16 O. V. Dolomanov, L. J. Bourhis, R. J. Gildea, J. A. K. Howard and H. J. Puschmann, *Appl. Crystallogr.*, 2009, **42**, 339–341.

17 A. L. Spek, *Acta Crystallogr., Sect. D: Biol. Crystallogr.*, 2009, **D65**, 148–155.

18 G. M. Sheldrick, *Acta Crystallogr., Sect. C: Struct. Chem.*, 2015, **C71**, 3–8.

19 C. F. Macrae, P. R. Edgington, P. McCabe, E. Pidcock, G. P. Shields, R. Taylor, M. Towler and J. van de Streek, *J. Appl. Crystallogr.*, 2006, **39**, 453–457.

20 (*a*) C. Lee, W. Yang and R. G. Parr, *Phys. Rev. B*, 1988, **37**, 785–789; (*b*) S. F. Boys and F. Bernardi, *Mol. Phys.*, 1970, **19**, 553–566; (*c*) S. Grimme, J. Antony, S. Ehrlich and H. Krieg, *J. Chem. Phys.*, 2010, **132**, 154104; (*d*) M. J. Frisch, G. W. Trucks and H. B. Schlegel *et al.*, Gaussian, Inc., Wallingford CT, 2016.

21 R. W. Seidel and R. Goddard, *Acta Crystallogr., Sect. C: Struct. Chem.*, 2015, **C71**, 664–666.

22 (*a*) S. Ebenezer, P. T. Muthiah and R. J. Butcher, *Cryst. Growth Des.*, 2011, **11**, 3579–3592; (*b*) G. Bolla, S. Mittapalli and A. Nangia, *IUCrJ*, 2015, **2**, 389–401; (*c*) S. Ranjan, R. Devarapalli, S. Kundu, S. Saha, S. Deolka, V. R. Vangala and C. Malla Reddy, *IUCrJ*, 2020, **7**, 173–183.

23 (*a*) A. Kálmán and L. Párkányi, *Isostructurality of Organic Crystals in Advances in Molecular Structure Research*, ed. M. Hargittai and I. Hargittai, JAI Press Inc, Greenwich, CT, USA, 1997, vol. 3, pp. 189–226; (*b*) K. K. Sarmah, K. Boro, M. Arhangelskis and R. Thakuria, *CrystEngComm*, 2017, **19**, 826–833.

24 (*a*) T. Gelbrich and M. B. Hursthouse, *CrystEngComm*, 2005, **7**, 324–336; (*b*) T. Gelbrich, T. L. Threlfall and M. B. Hursthouse, *CrystEngComm*, 2012, **14**, 5454–5464.

25 N. Schultheiss and A. Newman, *Cryst. Growth Des.*, 2009, **9**, 2950–2967.

© 2021 The Author(s). Published by the Royal Society of Chemistry

Open Access Article. Published on 15 September 2021. Downloaded on 4/7/2026 1:42:27 PM.
This article is licensed under a Creative Commons Attribution-NonCommercial 3.0 Unported Licence.

26 (*a*) M. K. Mishra, P. Sanphui, U. Ramamurty and G. R. Desiraju, *Cryst. Growth Des.*, 2014, **14**, 3054–3061; (*b*) P. Sanphui, N. R. Goud, U. B. R. Khandavilli and A. Nangia, *Cryst. Growth Des.*, 2011, **11**, 4135–4145.

27 E. Jurczak, A. H. Mazurek, Ł. Szeleszczuk, D. M. Pisklak and M. Zielińska-Pisklak, *Pharmaceutics*, 2020, **12**, 959.

28 (*a*) H. R. Guzmán, M. Tawa, Z. Zhang, P. Ratanabanangkoon, P. Shaw, C. R. Gardner, H. Chen, J. P. Moreau, Ö. Almarsson and J. F. Remenar, *J. Pharm. Sci.*, 2007, **96**, 2686–2702; (*b*) N. J. Babu and A. Nangia, *Cryst. Growth Des.*, 2011, **11**, 2662–2679; (*c*) M. Banik, S. P. Gopi, S. Ganguly and G. R. Desiraju, *Cryst. Growth Des.*, 2016, **16**, 5418–5428.

29 (*a*) X. Buol, K. Robeyns, C. C. Garrido, N. Tumanov, L. Collard, J. Wouters and T. Leyssens, *Pharmaceutics*, 2020, **12**, 653; (*b*) G. Kuminek, F. Cao, A. Bahia de Oliveira da Rocha, S. Gonçalves Cardoso and N. Rodríguez-Hornedo, *Adv. Drug Delivery Rev.*, 2016, **101**, 143–166.

© 2021 The Author(s). Published by the Royal Society of Chemistry